Production process monitoring and post-production strain measurement on a full-size carbon-fibre composite aircraft tail cone assembly using embedded optical fibre sensors

Edmon Chehura[1], Stephen W James[1], Stephen Staines[1], Chris Groenendijk[2], Denis Cartie[3], Stephanie Portet[4], Michael Hugon[4] and Ralph P Tatam[1]

[1] Engineering Photonics, Cranfield University, Bedfordshire, MK43 0AL Bedford, United Kingdom
[2] National Aerospace Laboratory (NLR), Composite Manufacturing Technology, Voorsterweg 31, 8316PR Marknesse, The Netherlands
[3] Coriolis Composites Technologies SAS, Z. A. du Mourillon, Rue Condorcet, F-56530 Queven, France
[4] DAHER Aerospace, 23 Route de TOURS, Saint Julien de Chedon, F41400 Montrichard, France

E-mail: r.p.tatam@cranfield.ac.uk

Abstract

Multiplexed optical fibre sensors were embedded into a carbon-fibre-reinforced-preform during the industrial production of a full-sized, one-piece tail cone assembly for a regional jet aircraft. Optical fibre Fresnel sensors monitored both the infusion of the resin, via measurement of the refractive index-dependent attenuation in the reflected light signal, and the degree of cure of the resin, via measurement of the chemical cure reaction-dependent change in refractive index. The resin cure was also monitored by optical fibre Bragg gratings (FBGs) fabricated in high linearly birefringent optical fibre, which measured through-thickness strain development, while FBGs in standard single mode optical fibre measured longitudinal strain development. The magnitudes and profiles of the transverse and longitudinal strains developed during the curing process were consistent across different locations on the tail cone. Typical transverse and longitudinal strains, related to cure reaction-induced shrinkage, were -1500 ± 17 µε and -500 ± 5 µε, respectively. Post-production, the same embedded FBG sensors were used subsequently to monitor structural strains when the tail cone was subjected to vacuum pressure loading. The longitudinal strains measured using the embedded FBG sensors were generally in good agreement with the longitudinal strains measured by the surface-bonded resistance foil strain gauge (RFSG) sensors, both qualitatively and quantitatively. The in-plane transverse and circumferential strains, oriented collinearly, were measured by the embedded FBGs and appropriately oriented surface-bonded RFSG sensors, respectively, and were, qualitatively, in good agreement.

Keywords: optical fibre sensors, carbon fibre composite material process monitoring, strain measurement

(Some figures may appear in colour only in the online journal)

1. Introduction

There has been a significant increase in the up take of composite material technology across a number of industries, thanks to the development of composite materials with innovative characteristics and to advancements in the manufacturing processes. Composite materials are lightweight and exhibit a large strength to weight ratio, making their use important for energy conservation in a range of applications. The aerospace industry alone has experienced major strides in the use of composite materials for aircraft structures, where, for example, Airbus (A380 and A350) and Boeing (787 Dreamliner) have pioneered commercial jet aircraft with significant carbon fibre reinforced polymer (CFRP) composite material content. Industrial scale production of composite material components does not, at present, incorporate sensors within the component to monitor the manufacturing process, and quality control is largely carried out empirically [1].

A number of non-optical methods are used for small scale, laboratory monitoring of some aspects of the manufacturing process [2]. Dielectric sensors are used to monitor resin flow, void content, viscosity and the degree of cure, by measuring the dielectric permittivity and loss factor (i.e. dielectric sensitivity) of the composite material between two or more electrodes that are excited by an alternating current [3, 4]. Direct current dielectric sensors are used to monitor resin flow and the degree of cure by sensing the electrical resistance between two electrodes [2, 5]. Ultrasonic transducers can also be used for monitoring resin flow, resin cure and void content [6], where the dependence of the ultrasonic wave velocity on the density and elastic modulus of the resin means that the time-of-flight through the composite preform will change with the progress of the cure reaction. Thermocouples and infrared thermometers can be used to monitor resin flow when there is a difference in temperature between the mould and the resin during the infusion process [7]. Pressure transducers, often based on the piezoresistive effect, are used for monitoring resin flow by transducing resin pressure into electrical resistance [8]. The use of these non-optical sensors is restricted to laboratory applications, as the sensors are either not suitable for embedding into carbonfibre reinforced composites, or are too large to be embedded into critical components without compromising the structural integrity.

Quality control in composites manufacturing processes could be facilitated by the use of embedded sensors that can provide real-time monitoring. Optical fibre sensors (OFS) are well suited to this application because they have many appropriate characteristics, including their small diameter, typically 40–125 µm. There are five categories of OFS that have been explored for monitoring the processing of composite materials; evanescent field sensors, Fresnel sensors, interferometric sensors, grating sensors and spectroscopic sensors. Resin infusion and cure can be monitored using sensors that are sensitive to changes in the refractive index of the surrounding medium. The arrival of resin at a location can thus be detected as the surrounding medium changes from air to resin with a concomitant significant increase in refractive index, and the refractive index

of the resin is known to be correlated with the degree of cure of the resin [9, 10]. The perturbation of the evanescent field of the electromagnetic wave propagating in the core of the optical fibre can also be used to detect changes in the refractive index of the surrounding medium, exploiting etched [11, 12], tapered [13, 14] and side polished optical fibres [15]. Alternatively, the refractive index dependence of the Fresnel reflection from a cleaved fibre end [10, 16–19] can be exploited. Optical fibre interferometers, such as the extrinsic Fabry–Perot interferometer, have been used to monitor the development of internal strains during the curing of a composite [20]. The infusion, flow and cure of resin can also be monitored using optical fibre grating sensors such as fibre Bragg grating (FBG), tilted fibre Bragg grating (TFBG) and long period grating (LPG) sensors [10, 21–25]. Grating sensors can be configured to perform multi-parameter sensing, which is useful for the simultaneous measurement of strain and temperature [26–29]. Optical fibre based spectroscopic sensors can be embedded into the composite to determine the degree of cure by monitoring chemical changes caused by the cure reaction [30, 31].

In this work, a full-scale, one-piece aircraft tail cone assembly has been made from wholly composite material using industrial-scale manufacturing processes. Dry carbonfibre placement onto a uniquely designed one-piece tool was automated using a pre-programmed robotic machine. The tool facilitated the incorporation of 10 stringers in the preform, which were reinforced through-the-thickness by tufting [32, 33], using an automated robotic machine, prior to resin infusion and cure processes. The work investigated the feasibility and challenges of incorporating embedded OFS into the carbon-fibre-reinforced-preform (CFRP) to monitor the manufacturing processes, from lay-up of the preform through resin infusion and cure, to post-fabrication strain measurements. The well-known challenges include the harsh environment, the complexity of implementing ingress/egress connection schemes [34] and the requirement to maintain vacuum pressure when sensors are embedded [35]. The embedded OFSs were fabricated in single mode (SM) and high linearly birefringent (HiBi) optical fibres. Multiplexed optical fibre Fresnel, SM FBG and HiBi FBG sensors monitored the infusion of resin, resin cure and the development of strain in the longitudinal and transverse directions at various locations within the tail cone. Post-production, the embedded fibre grating sensors, along with surface-mounted resistance foil strain gauge (RFSG) rosettes, were used to monitor structural strains when the tail cone was subjected to vacuum pressure loading.

2. Principles of optical fibre sensors

2.1. Optical fibre Fresnel sensor

The cleaved end of an optical fibre forms an optical fibre Fresnel sensor, as shown in figure 1(a). Light propagating along the optical fibre and incident on the fibre end is partially reflected, with the reflectivity being dependent on the refractive index of the external medium, as illustrated by figure 1(b). The ability of the Fresnel sensor to monitor changes in refractive index
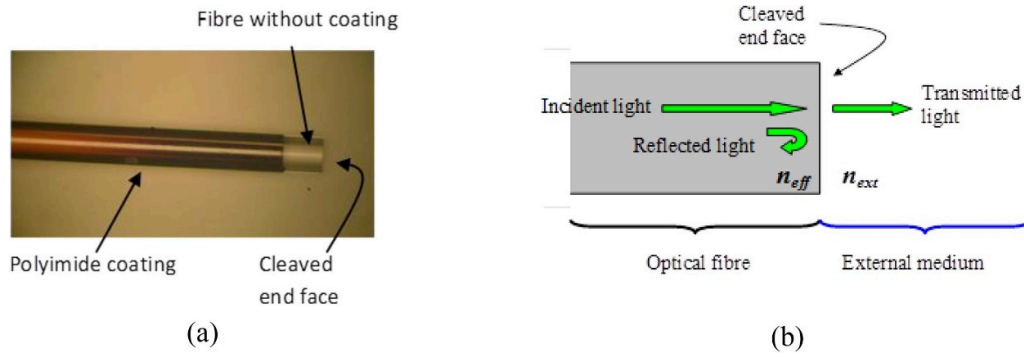
Figure 1. Optical fibre Fresnel sensor element (a) image of sensor and (b) sensing principle. n_{eff}; effective refractive index of the optical fibre, n_{ext}; external refractive index. The diameters of the optical fibre (FX-PI-01-01-01, Fibertronix), with and without the polyimide coating, are 135 and 125 μm, respectively.

makes it a suitable candidate for monitoring resin infusion and cure.

The refractive index of the medium surrounding the Fresnel sensing element can be determined by monitoring the power reflected from the fibre-end. However, the reflected power is also influenced by light source fluctuations, down-lead perturbations and the thermo-optic property of the optical fibre, which necessitates the use of a reference channel that compensates for these effects. In this work, the reference channel consisted of a cleaved fibre end that experienced the same temperature environment as the Fresnel sensing element but that was deployed such that the surrounding medium was air (see section 2, figure 3). The refractive index of the surrounding medium measured by the Fresnel [36] sensor is given by equation (1) [10, 37], where n_{eff} is the effective refractive index of the propagating mode and n_{ext} is refractive index of the external material. In equation (2), n_a is the refractive index of air, V_{air} is the voltage produced by the photo-detector that monitors the reflected intensity from the reference fibre end and V_{ext} is the voltage produced by the photo-detector that measures the reflected intensity from the sensing Fresnel element:

$$n_{\text{ext}} = n_{\text{eff}} \cdot \frac{1 - \frac{\Delta}{\sqrt{R}}}{1 + \frac{\Delta}{\sqrt{R}}}, \tag{1}$$

$$\Delta = \frac{n_{\text{eff}} - n_a}{n_{\text{eff}} + n_a} \text{ and } R = \frac{V_{\text{air}}}{V_{\text{ext}}}. \tag{2}$$

2.2. Fibre Bragg grating sensors

An FBG is a periodic refractive index modulation inscribed into a short section (typically of length 1–5 mm) of the core of an optical fibre by exposure to, for example, a spatially modulated intensity pattern from a UV laser beam [38]. When light from a broadband source, or a tuneable laser, is coupled into the optical fibre, the FBG reflects light within a narrow wavelength band, typically 0.5 nm, back towards the source, with the central wavelength being dependent upon the period of the grating. The reflected spectrum from an FBG fabricated in SM optical fibre (figure 2(a)), where refractive index

in the core is isotropic, is a single peak (figure 2(c)). HiBi optical fibre is fabricated such that its core has an anisotropic refractive index. An FBG fabricated in HiBi fibre exhibits two reflected peaks that are separated by typically 0.3 nm (figure 2(d)) [39–43]. The HiBi FBG reflection peaks correspond to the two orthogonal polarisation Eigen-axes of the fibre, the fast and slow axes [39–42]. The operation of FBGs as sensor elements is based upon measurement of changes in the reflected Bragg spectrum caused by physical perturbations such as strain and temperature that interact with the FBG by modifying its refractive index and/or its periodicity. The FBG sensor's ability to detect physical measurands such as strain, pressure and temperature has been exploited previously in the monitoring of composite material processing [44, 45]. In this work, cure-induced strains directed along and transverse to the optical fibre have been monitored using SM FBG and HiBi FBG sensors, respectively.

The change in temperature, ΔT, and longitudinal strain, $\Delta\varepsilon$, measured by an SM FBG sensor can be calculated from equations (3) and (4) respectively, where λ_B is the reflected Bragg wavelength. $\Delta\lambda_B$, K_T and K_ε are the Bragg wavelength shift, and the temperature and strain responsivities of the FBG, respectively:

$$\Delta\lambda_B = K_T \cdot \Delta T, \tag{3}$$

$$\Delta\lambda_B = K_\varepsilon \cdot \Delta\varepsilon. \tag{4}$$

In this work, the Bragg wavelength shift exhibited by the SM FBG sensors is interpreted as longitudinal strain by using equation (4) [35, 46], after compensating for the temperature dependence of the Bragg wavelength, which was determined using equation (3) and temperature measurements provided by a thermocouple probe. The responsivities of the SM FBG to longitudinal strain and to temperature were calibrated by measuring changes in the Bragg wavelength as a function of temperature in the absence of strain and as a function of an applied strain at room temperature, respectively.

A HiBi FBG sensor reflects the Bragg wavelengths, $\lambda_{B,f}$ and $\lambda_{B,S}$, along the fast and slow axes, respectively, as a consequence of the fibre having effective refractive indices, $n_{\text{eff},f}$
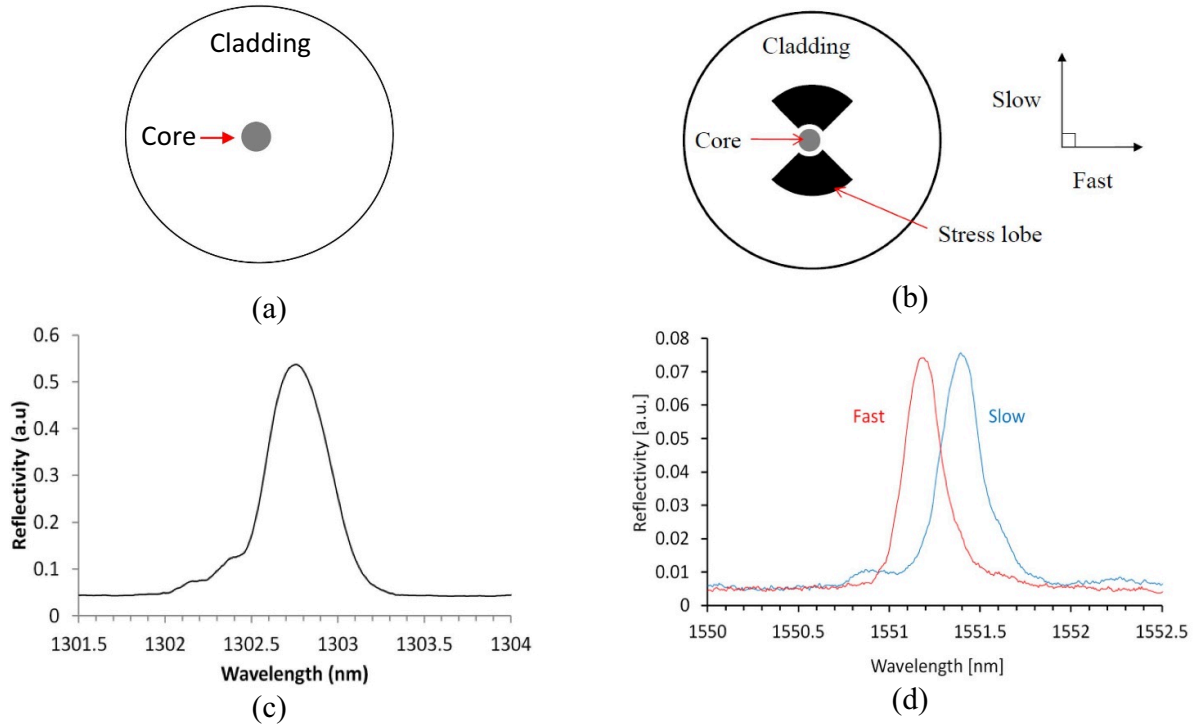
Figure 2. Cross-section of (a) SM and (b) HiBi optical fibres, and the spectra reflected by an FBG fabricated in (c) SM and (d) bow–tie HiBi optical fibres, respectively. Fast and slow refer to the polarisation Eigen axes of the HiBi optical fibre.

and $n_{\text{eff,S}}$, along the fast and slow axes, respectively. Loading the optical fibre transverse to its longitudinal axis results in a change in the birefringence of the optical fibre, which causes differential shifts in the Bragg wavelengths of the reflections from the orthogonally polarised Eigen modes. If the HiBi FBG is subjected simultaneously to three normal components of strain and to temperature, it is not possible to discern the four unknown measurands from a measurement of the two Bragg wavelengths of the HiBi FBG. Equation (5) was derived previously to obtain an effective transverse strain component, by using an analysis that compensates for 2 of the measurands [39, 40]. This effectively cancels out the longitudinal strain contribution to the wavelength shift, while the contribution to the wavelength shift due to the temperature is compensated by using the temperature history measured by, for example, a thermocouple probe:

$$\varepsilon_{\text{transverse}} = \frac{2}{n_o^2 \left(p_{12} - p_{11}\right)} \left[\frac{\Delta\lambda_f}{\lambda_{B,f}} - \frac{\Delta\lambda_s}{\lambda_{B,s}}\right]. \quad (5)$$

In equation (5), s and f denote the slow and fast axes, respectively, $\lambda_{B,i}$ ($i = s, f$), are the two orthogonally polarised Bragg wavelengths at quiescent conditions, $\Delta\lambda_s$ and $\Delta\lambda_f$, are the wavelength shifts of the Bragg peaks, n_o is the average refractive index and the constants $p_{11} = 0.113$ and $p_{12} = 0.251$ are the Pockels strain-optic coefficients of the optical fibre. When the values of n_o, p_{11} and p_{12} are known for the HiBi FBG sensor, the effective transverse strain can be determined using equation (5) [39]. The responsivity of the HiBi FBG wavelengths to temperature was calibrated

by measuring changes in the Bragg wavelengths as a function of temperature in the absence of strain, as discussed earlier.

In this work, all FBG sensors were fabricated by exposing the optical fibre to the output from a frequency-quadrupled flashlamp-pumped Nd:YAG laser, operating at 266 nm, through a phase mask [47]. The SM FBGs were fabricated in optical fibre from Fibertronix, FX-PI-01-01-01, while the HiBi FBGs were fabricated in optical fibre from Fibercore, HB1250P. Both types of optical fibre were polyimide coated, facilitating high temperature operation. The fibres were, prior to FBG fabrication, soaked in hydrogen for 2 weeks at room temperature and with the gas pressure maintained at 100 bars, in order to photosensitise the fibre core.

2.3. Instrumentation: Fresnel refractometer

Figure 3 shows a schematic diagram of a Fresnel refractometer that was configured with eight spatially multiplexed sensing elements and that was used to monitor the infusion of resin and to measure subsequently the refractive index of the resin at eight different locations in a sample. The 'Air reference' channel was used when performing quantitative measurements of the refractive index of the resin during the cure process, and was described in section 2.1. A portable instrument based on the schematic shown in figure 3 was constructed. The outputs from the photodiodes were monitored in real-time on a computer via a data acquisition system comprised of an external chassis (NI PXI-1033) containing two multiple-channel lock-in amplifier electronic boards (NI PXI-4462).
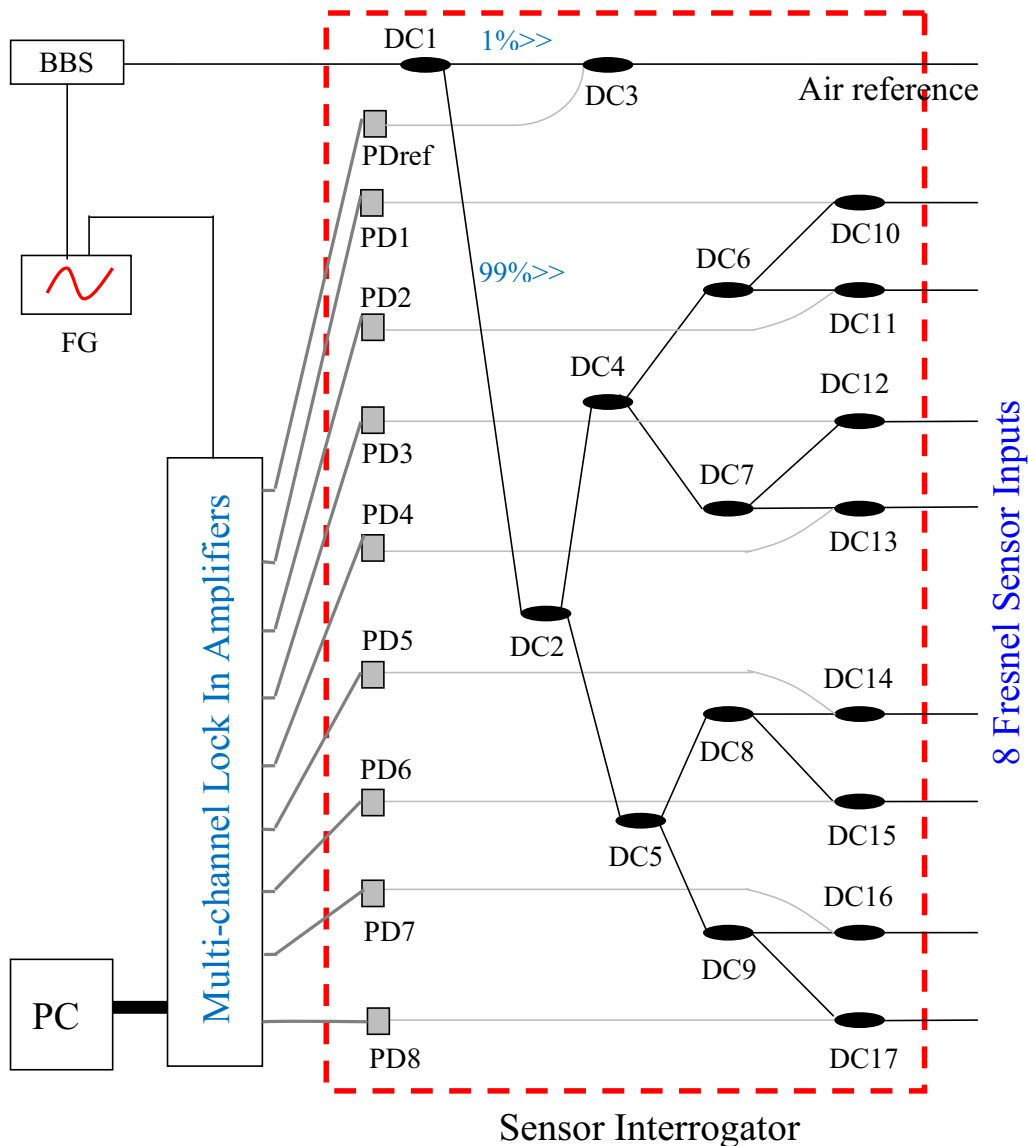
Figure 3. Schematic of the instrumentation consisting of 8 multiplexed Fresnel sensors and a reference Fresnel sensor. BBS; broadband light source with 100 nm bandwidth centred at 1550 nm and 15 mW out power (Covega SLD 1005), DC1–DC17; directional couplers, PD$_{ref}$ and PD1–PD8; photodetectors (New Focus, 2011-FC), FG; function generator (Stanford Research Systems, DS345), PC; personal computer. DC1 has a split ratio of 99/1, while all other of directional couplers have a 50/50 split ratio.

2.4. Instrumentation: fibre Bragg grating interrogators

Separate instruments were designed and constructed to interrogate the SM and HiBi FBG sensors. The HiBi FBG interrogator employed birefringent optical fibre components and a custom-made swept laser source (Santec, HSL 2000), which scanned across a 49 nm bandwidth centred at 1287 nm at a fixed scan rate of 2.5 kHz. The degree of polarisation of the laser is 99% and the coherence length is 30.5 mm (table 1). A fibre polariser, having 28 dB extinction ratio, was connected to the output of the laser such that it equally populated the Eigen modes of the subsequent PM components. A schematic diagram of the instrument is shown in figure 4, which is based on the system reported in [42], but expanded to allow the interrogation of four HiBi FBG sensor arrays. The instrument was configured with fibre polarisation splitting and

polarisation maintaining couplers to allow the interrogation of the reflections from each polarisation Eigen-mode independently and simultaneously, using separate photo-detectors. Figure 5 shows the spectrum of an array of five wavelength division multiplexed HiBi FBGs interrogated using this system.

The SM FBG interrogator employed a commercially-available swept laser source, Santec, HSL 2000, with a 110 nm wavelength bandwidth centred at 1318 nm, 20 mW output power and a fixed scan rate of 20 kHz, and was configured with SM fibre components, as shown in figure 6, to monitor 4 arrays of SM FBGs simultaneously. The degree of polarisation of the laser is 99% and the coherence length is 6 mm (table 1). Also shown is the input from the broadband light source (BBS) of 100 nm bandwidth centred at the wavelength of 1550 nm, which was used to interrogate the Fresnel sensors that were located at the distal ends of the optical fibres containing the SM

Table 1. Summary of the light sources used and their characteristics.

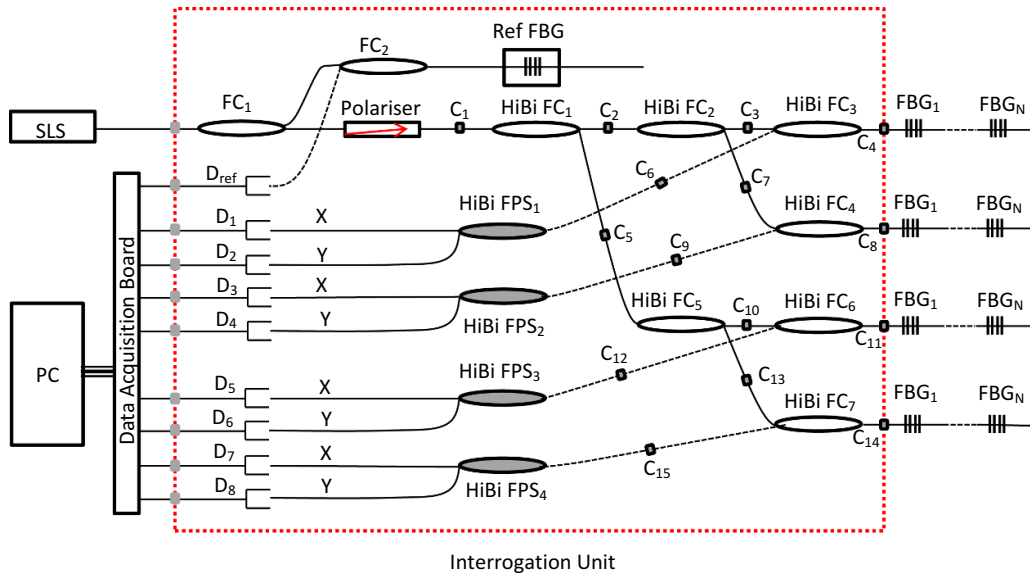| Light source	Model	Output power (mW)	Centre wavelength (nm)	Wavelength range (nm)	Coherence length (mm)
Broad band	Covega SLD 1005	15	1550	100	0.02
Swept laser (2.5 kHz)	Santec, HSL 2000	20	1287	49	30.5
Swept laser (20 kHz)	Santec, HSL 2000	20	1318	110	6

Figure 4. Schematic of the instrument used to interrogate the HiBi FBG sensors. SLS; swept laser source (1300 nm wavelength), FC; single mode fibre coupler, HiBi FC; HiBi fibre coupler, FBG; HiBi FBG, C_{1-15}; adjustable HiBi connectors, HiBi FPS; HiBi fibre polarisation splitter, D; detector, X/Y; orthogonal polarisation states, PC; personal computer, Ref FBG; reference single mode FBG.
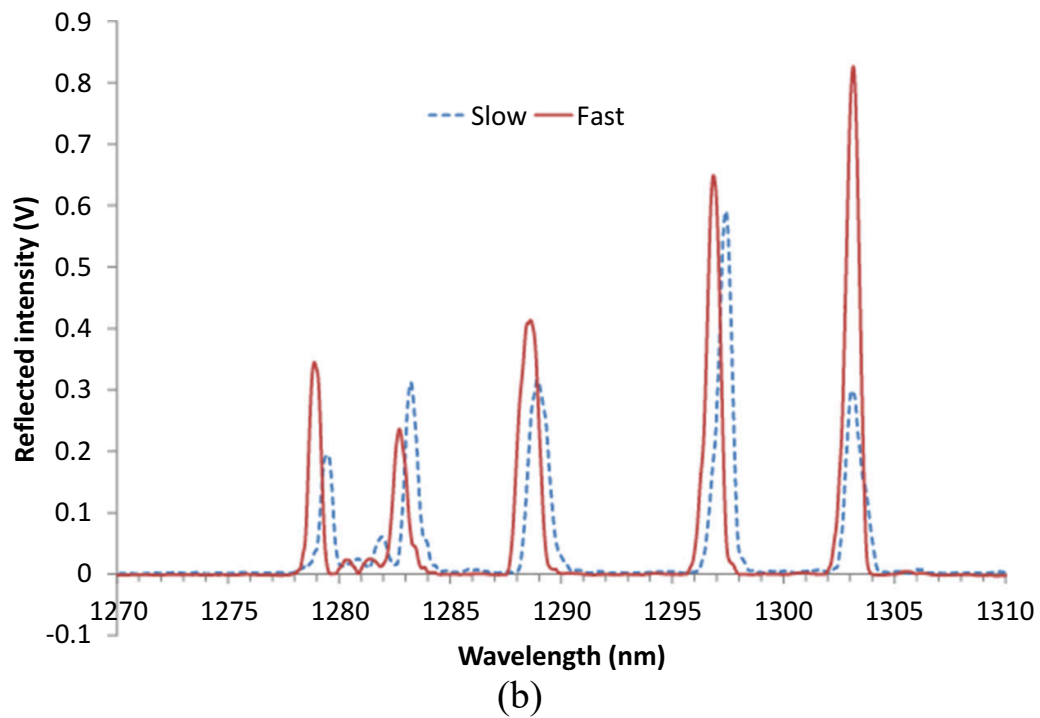

(b)

Figure 5. Five wavelength multiplexed FBG sensors fabricated in HiBi (Fibercore, HB1250P) optical fibre, recorded using the system shown in figure 4 when the FBGs were at quiescent conditions. The two Bragg peaks at 1303 nm appear co-located because of the external birefringence imposed by the bending and twisting of the fibre array at the distal end location of this FBG on a length of fibre too long (>4 m) to be kept straight on the table.
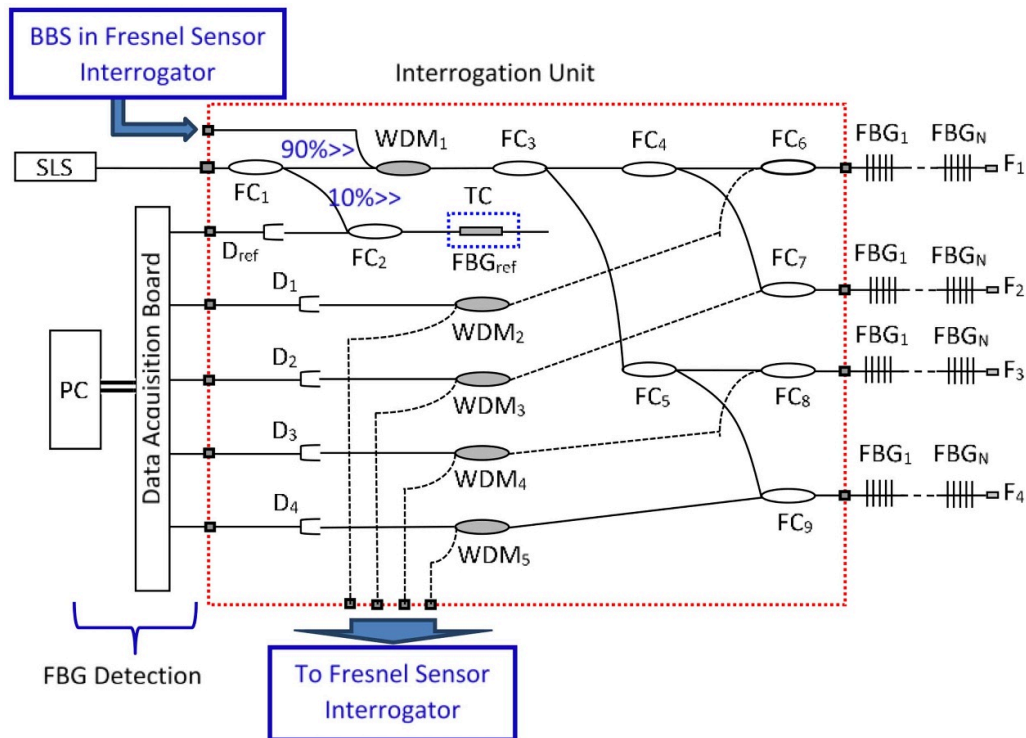
Figure 6. Schematic of the instrument used to interrogate the SM FBG sensors and to interrogate the Fresnel sensors formed at the distal ends of the fibres. SLS; swept laser source at 1300 nm, FC; single mode fibre coupler (50/50 split ratio), BBS; broadband sources at 1550 nm, FBG; SM FBG, D; detector, F; Fresnel sensor at distal end, PC; personal computer, Ref FBG; reference single mode FBG, TC; temperature controlled, WDM; wavelength division multiplexer for wavelengths of 1300 nm (SM FBG sensors) and 1550 nm (Fresnel sensors).
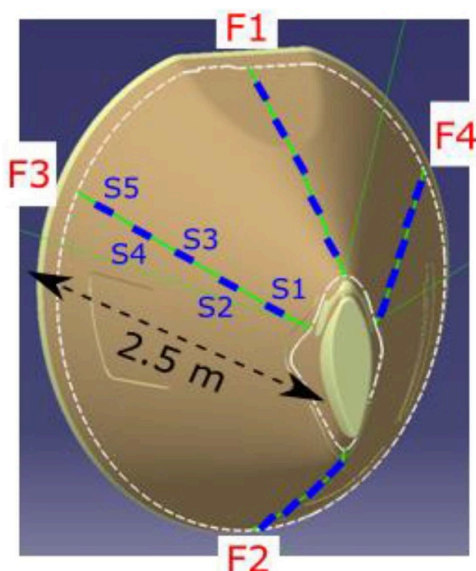

Figure 7. 3D drawing of the rear view of the tail cone exterior showing optical fibre sensor locations S1–S5 within each of the zones F1–F4 of the tail cone. The separation between sensors in each array is 40 cm. The length, largest and smallest diameters of the tail cone are 2.5 m, 1.6 m, and 0.5 m, respectively.

FBG sensors. WDM couplers (1550/1300 nm) were used to separate the reflections from the Fresnel and SM FBG sensors. The strains measured by the SM FBG sensors were interpreted

as longitudinal strains by using equation (4) [46], after compensating for the temperature response of the Bragg peak, as described in section 2.2.

For both FBG interrogators, data sampling was performed at 100 MS s^{-1}. As such high data rates were unnecessary for the cure monitoring process, the acquired data were subsequently down sampled and averaged to an equivalent scan rate of 100 Hz.

3. Preform and sensor lay-up, and tufting

The full-size carbon-fibre-reinforced tail cone assembly was designed for an Embraer regional jet aircraft. Figure 7 shows the design of the tail cone, which contained three doors/windows and 10 stringers, incorporated to provide added stiffness, on the interior. The dimensions of the tail cone were 2.5 m, 1.6 m and 0.5 m for the long axis and for the largest and the smallest diameters, respectively. The tool on which the tail cone assembly was moulded was constructed by Recomet Impex (Romania). The assembly of the carbon fibre onto the tool and the integration of the optical fibre sensors were performed at Coriolis Composites (Lorient, France) using automated dry fibre placement (ADFP) implemented by an industrial robotic system (figure 8) [48]. The tool, containing the tail cone assembly, was subsequently transported to Cranfield University (Bedford, UK) where through-thickness reinforcement of the stringers was performed by tufting [18, 31]. The
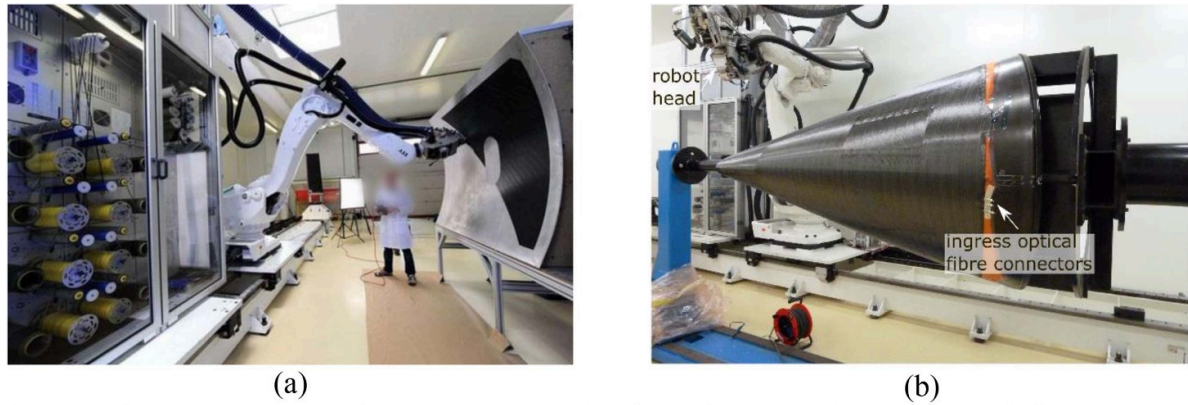
Figure 8. (a) Robotic system for the automatic dry fibre placement (ADFP) at Coriolis Composites and (b) a 90° ply of dry carbon fibre being laid after the optical fibre sensors had been laid. Figure (b) also shows the location of the ingress/egress fibre connectors.

Table 2. Specification of the optical fibres in which the sensors were fabricated.

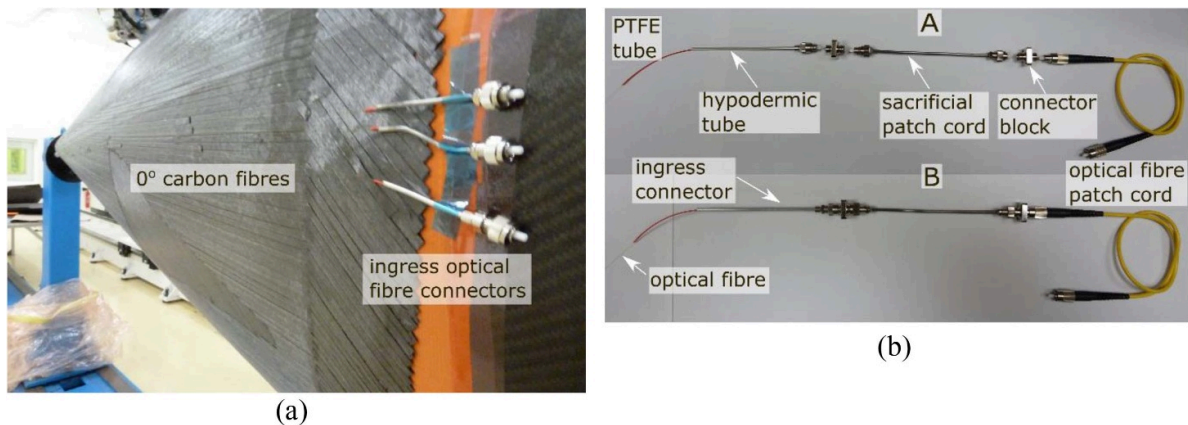| Fibre type	Manufacturer	Fibre identification number	Coating type	Core diameter (µm)	Cladding diameter (µm)	Total diameter (µm)
SM	Fibertronix	FX-PI-01-01-01	Polyimide	9	125	135
HiBi	Fibercore	HB1250P	Polyimide	6 ± 0.2	125 ± 2	145 ± 5

Figure 9. (a) Optical fibre sensors were laid onto the 3rd ply such that they were oriented parallel to the 0° carbon fibres. (b) Photograph of the ingress connector and the sacrificial patch cord for connection to the embedded optical fibre sensors and to the interrogating instruments. A and B in (b) show the configuration of the connection system before and after connecting the components together, respectively.

tail cone assembly was then transported to DAHER Aerospace (Nantes, France) where it was infused with liquid resin and subsequently cured. After manufacture, the tail cone assembly was demoulded from the tool and was transported to the National Aerospace Laboratory (NLR) in the Netherlands where the tail cone was subjected to pressure loading.

A total of seven plies of dry carbon fibre were laid to form the main body of the tail cone structure (figure 7) using ADFP. The orientation of the plies from the underside to the upper surface was 45°/−45°/0°/90°/0°/−45°/45°, where the 0° ply was aligned with the long axis of the tail cone. Optical fibre sensors were embedded in the tail cone in 4 zones, denoted as F1–F4 in figure 7. Zones F1 and F2 coincide with the shortest (2.3 m) and longest (2.5 m) dimensions, respectively, of the tail cone. The sensors were embedded after the first three plies had been placed on the tool.

The optical fibres were hand-laid onto the 0° oriented ply, after which four more plies were added (figure 8). The orientation of the sensors in zones F3 and F4 were displaced so that the optical fibres avoided the stringers and doors, and the sensors were therefore laid crossing the 0° ply fibres at an angle <2°. Each of the zones F1–F4 contained three embedded optical fibres; one SM fibre with a Fresnel sensor at its distal end, one SM fibre containing five equally-spaced FBG sensors, and one HiBi fibre containing five equally-spaced FBG sensors along the fibre length (the sensors are described in more detail in section 5.2). The physical spacing between the FBGs in each array was 400 mm. The embedded SM FBGs and HiBi FBGs were each placed in the middle of separate carbon fibre tapes that were laid adjacently, and the width of each carbon fibre tape was 6.35 mm. Polyimide coated fibres were used to ensure that the buffer coating withstood the
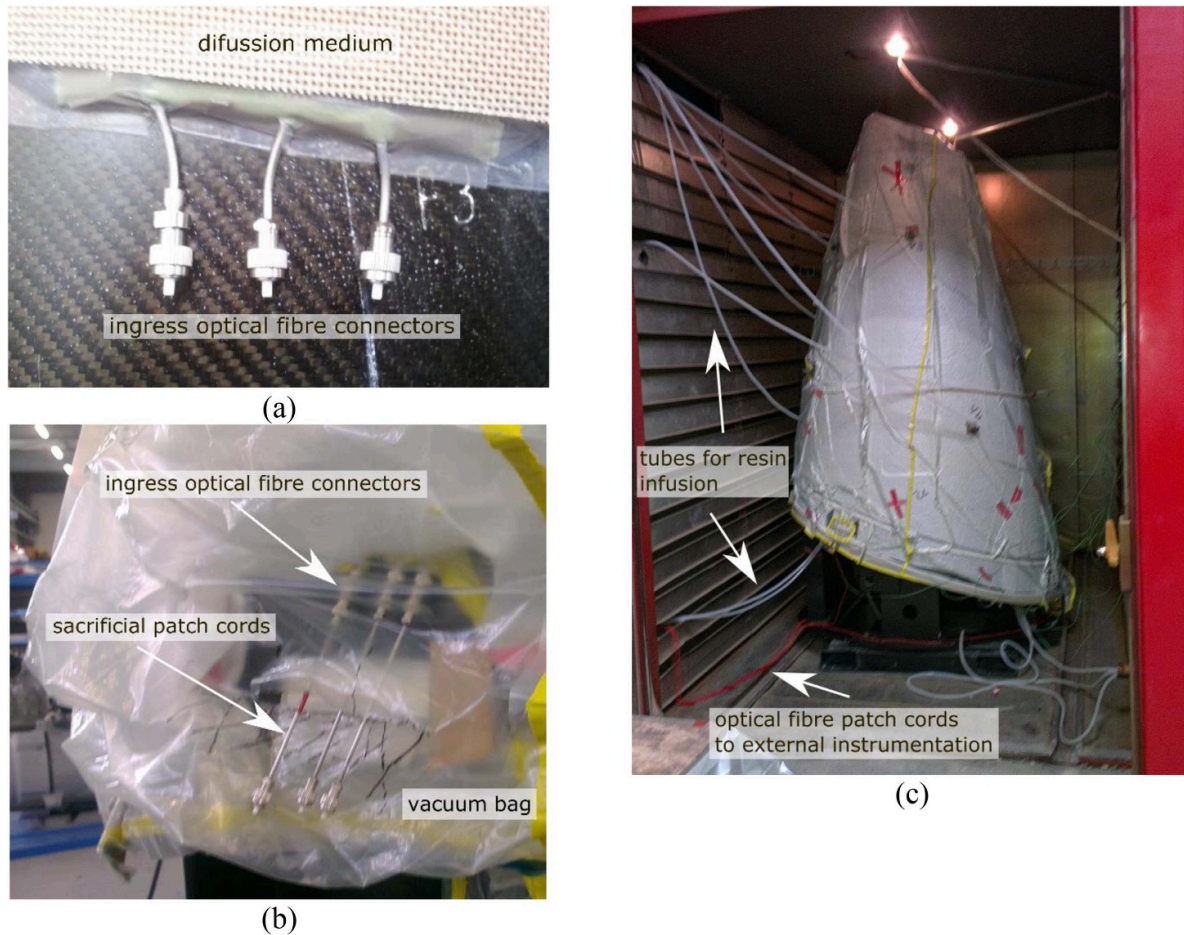
Figure 10. (a) Ingress/egress optical fibre connector ends before the vacuum bag installation; (b) sacrificial patch cords connected to ingress connectors allowing the installation of vacuum bags; and (c) tail cone preform fixed upright in the oven ready for resin infusion and cure. The purpose of the diffusion medium is to spread the resin uniformly over the preform during the infusion process.

temperatures, up to 180 °C, used when curing the composite material. The details of the optical fibres used are shown in table 2.

The output from a CO_2 laser was used to remove the polyimide coatings from the distal ends of the optical fibres, and from the sections of the fibres in which the FBGs were fabricated. Each FBG, 2 mm long, was centred on a stripped fibre section of length 3 mm. The FBGs were not re-coated following inscription. The FBG sensors along the lengths of the optical fibres are denoted from S1 to S5 in figure 7. The distal end of each optical fibre containing SM FBG sensors was also used as a Fresnel sensor.

Hand-layup of the optical fibre into the structure was necessary to allow accurate positioning of the sensors within the part and to ensure the appropriate orientation of the polarisation Eigen-axes of the HiBi FBGs with respect to the principal directions (in-plane and out-of-plane) of the tail cone. The orientations of the polarisation Eigen-axes were marked with tape after they had been identified by the observation of the diffraction pattern from the side of the optical fibre when illuminated by a laser beam in the visible wavelength spectrum [41]. The measurements made by the HiBi FBGs are thus of transverse strains that are in-plane or out-of-plane [39, 40] of the

tail cone, while the measurements from the SM FBG sensors were interpreted as longitudinal strain. The tail cone preform was reinforced in the through-thickness direction, after layup, by means of tufting at the feet of the stringers, 10 in total, all in the interior of the tail cone. The on-line monitoring of the strains experienced by the needle during the tufting process were also performed using multiplexed SM FBG sensors which were surface-bonded to the needle [18, 31].

The ingress/egress points of the embedded optical fibres were located on the edge of the preform at the fuselage end of the tail cone. Figure 9 shows the design of the ingress connections. A stainless steel hypodermic tube was used to protect the ingress of the optical fibre. The hypodermic tube withstands pressure loads in excess of 2.5 bar, which are greater than the pressure exerted by the robot head during the ADFP process. Additional protection to the optical fibre inside the hypodermic tube was provided by PTFE tubing. The length of the hypodermic tubing used at the ingress was 70 mm, of which 30 mm was embedded in the edge of the preform. An optical fibre of length l50 mm, protected by PTFE tubing and a hypodermic tube, was terminated with FC/PC connectors on both ends to form a sacrificial fibre patch cord. The sacrificial fibre patch cord provided an agile link between the embedded

sensors and the interrogating instruments located external to the oven, and was designed to ease the process of installing the vacuum bags over the tail cone preform for implementing the infusion and cure processes, and to ensure that the vacuum pressure required for the infusion of resin was not compromised. Two connector blocks were used to connect the sacrificial patch cords to the fibre sensors on one end and to the instrumentation on the other end. The sacrificial patch cords were made from SM and HiBi optical fibres, where the appropriate orientations of the polarisation Eigen-axes were configured by viewing the fibre end through an optical microscope (Olympus BX51) to $\pm 2°$ accuracy.

4. Infusion monitoring

Figure 10 shows the installation of the vacuum bags over the tail cone preform in preparation for the resin infusion and cure processes and illustrates the role of the sacrificial patch cords in enabling installation of the vacuum bag and in connecting the sensors to the external instrumentation. During the infusion and cure processes, the tail cone was placed upright in the oven, with the exhaust-end located at the top. A total of seven thermocouple probes were attached to the surface of the tail cone, spatially distributed on the outside surface of the tail cone preform. The thickness of the carbon fibre preform between the embedded FBGs and the surface to which the thermocouples were attached was ~1.5 mm. For such a small thickness, and with the assumption that the interior of the temperature furnace containing the tail cone was in thermal equilibrium, the temperature gradient was considered insignificant.

As the infusion of the resin was to be performed against gravity, the knowledge of the arrival of resin at various heights of the tail cone was important, requiring the distribution of the sensors along the height of the tail cone. The process of infusion was performed against gravity so as to facilitate uniform coverage of the tail cone preform with resin, otherwise an infusion carried-out parallel to gravity will cause the bottom parts of the tail cone preform to saturate more with resin [49, 50]. The resin infusion into the tail cone preform was monitored by Fresnel sensors which were embedded such that two sensors were located (one half-way up and the other at the top of the tail cone) in each of the four zones indicated as F1–F4 in figure 7. The nomanclature adopted for the Fresnel sensors is Fi_h and Fi_t, where $i = 1$–4 represents the zone in which the sensor is embedded, while h and t represent sensors located half-way up and at the top of the tailcone, respectively. Figure 11 shows the data recorded from a selection of the sensors during resin infusion. The significant attenuation in the reflected signal that ocurs when the resin (refractive index = 1.54 at 1550 nm) covers the Fresnel sensor was used to identify the arrival of resin at a sensor.

Sensor F3_h, embedded half-way up the length of the tail cone in zone-F3, detected the resin 24 min after the infusion process was started. This was 1.5 min before the resin was detected by sensor F1_t, which was located close to the
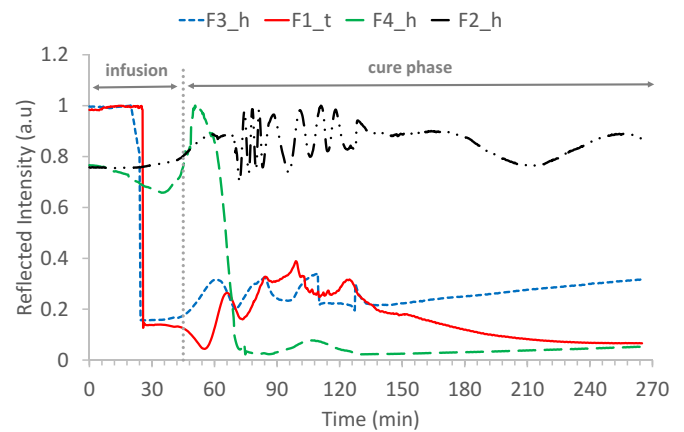

Figure 11. Resin infusion into the tail cone assembly detected by three of the Fresnel sensors located in different zones of the tail cone preform. The Fresnel sensors, F3_h and F4_h, embedded in zone-F3 and zone-F4 respectively (see figure 7), were located half way up the tail cone while F1_t, embedded in zone-F1, was located near the exhaust end (top of tail cone). The resin arrival times at the three sensors were 24, 25.5 and 55 min respectively, from the start of the infusion process. Fresnel sensor F2_h, located half way up the tail cone in zone-F2, shows effectively an unaltered signal during the infusion of resin. The Fresnel sensors have been labelled according to the tail cone zones in which they were embedded. The initial reflected intensities, before the infusion process and before the arrival of resin at the sensors after starting the infusion, is depicted by the first ~20 min.

exhaust-end (top) of the tail cone in zone-F1. This was expected, as the resin inlet was located at the bottom of the tail cone. Fresnel sensor F4_h, embedded half-way up the tail cone in zone-F4, detected the resin 15 min after the infusion process was stopped, which was after the cure thermal profile was started. This suggests that the resin had not infused into every part of the preform by the time the infusion process was terminated. The viscosity of the resin decreases when the temperature is increased, which consequently assists the flow and the spreading of the resin further into the preform. One of the sensors, F2_h, did not detect resin, suggesting the existence of a resin void. As the active region of each Fresnel sensor element corresponds to the mode field diameter of the fibre propagating mode (approximately 9 µm in diameter), local resin pockets of microscopic size can be detected. In figure 11, the Fresnel sensor signals in the time range from ~45–135 min are characterised by a modulation that could be attributed to movement and bending of the sensor element within the preform, as perturbations on this part of the optical fibre down lead are not corrected by the intensity referencing.

5. Cure monitoring

Two methods were used to monitor the curing of the resin. Firstly, the change in the refractive index of the resin caused by the chemical cure reaction was monitored using the optical fibre Fresnel sensors embedded within the preform. Secondly,
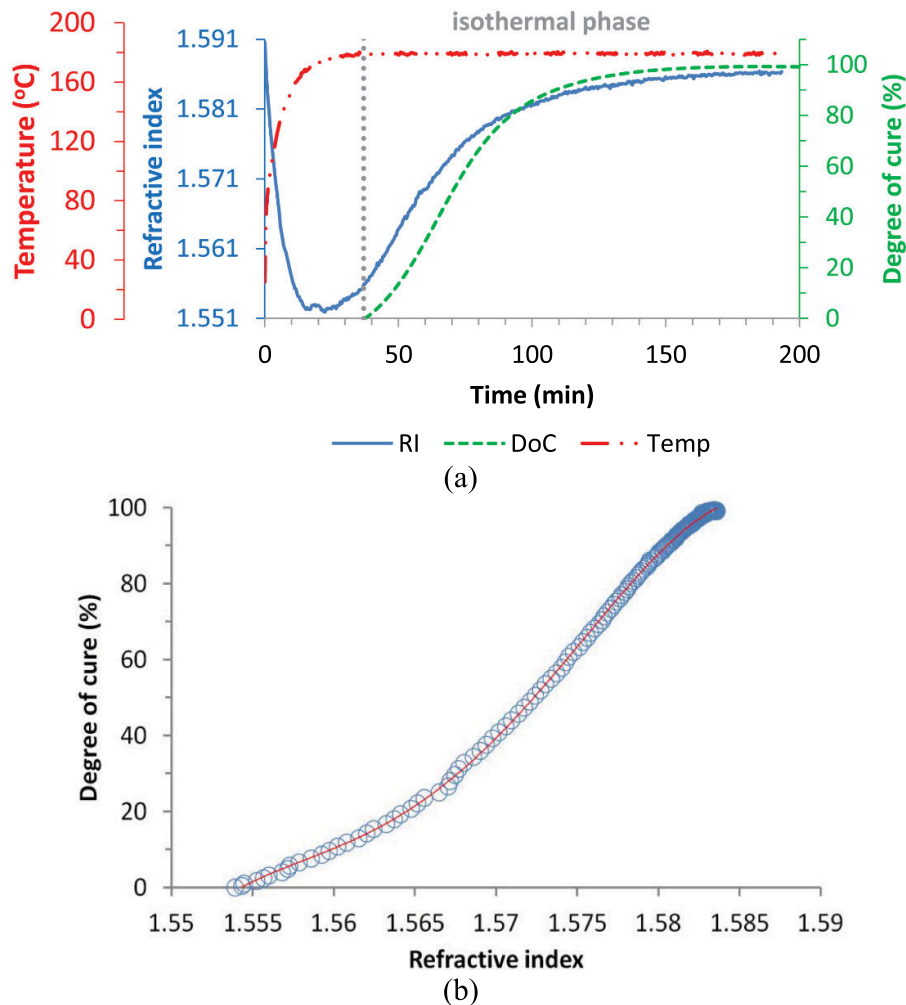
Figure 12. (a) Calibration of the Fresnel refractive index measurement against the degree of cure determined by the DSC for a neat resin (EP2400 resin), with the red line showing the temperature, the blue line showing the refractive index and the green line the degree of cure. (b) Correlation function (cubic) for the calibration over the isothermal temperature of 180 °C. The dotted line in (a) marks the time, 37 min, at which the correlation of (b) was started. The circles in (b) represent data points and the solid line is a cubic fit. RI, refractive index; DoC, degree of cure; Temp, temperature.

the strains developed within the preform during the curing of the resin were monitored using the embedded FBG sensors.

5.1. Optical fibre Fresnel sensor

The refractometer, after monitoring the infusion of the resin, was used to subsequently monitor the change in refractive index of the resin during the cure cycle, which was determined in real time using equation (1). The calculated refractive index can be directly converted into the degree of cure of the resin, provided the refractive index measurement from the Fresnel sensor had been calibrated against the degree of cure obtained using differential scanning calorimetry (DSC) [51]. There are also formulae for determining the degree of cure of a resin system [52].

The information pertaining to the degree of cure and cure cycle of the RTM6 resin that was used in the manufacture of

the tail cone is not provided in this publication as it is confidential to the industrial partners. Instead, to illustrate the methodolody that was employed, the process of calibration of the sensor and an example of its use in a planar CFRP panel using a different resin system and cure cycle is described [53]. Figure 12 shows a typical calibration curve obatined for the resin system (EP2400), which was established by monitoring the refractive index and the heat of reaction of a sample of curing neat resin measured by the Fresnel sensor and the temperature-modulated DSC [30, 31], providing the relationship between refractive index and degree of cure. The cure cycle for the calibration experiment consisted of two parts, the dynamic part during which the temperature was increased rapidly, and the isothermal part during which the temperature was held constant at 180 °C (figure 12(a)). The data in the initial part of figure 12(a) (<30 min), in which the refractive index decreased with the increase in temperature, were attributed to the thermo-optic property of the *resin*, since the contribution

from the thermo-optic property of the *optical fibre* was compensated by the referencing scheme. The increase in refractive index under isothermal conditions is associated with the chemical cure reaction [9, 10, 54]. The refractive index measured during the isothermal phase of the cure was used to determine the correlation between the change in refractive index and the degree of cure of the resin, which is plotted in figure 12(b).

A Fresnel sensor, employing the correlation function determined from the calibration shown in figure 12(b), was used to convert, in real time, the refractive index measurement (figure 13(a)) into the degree of cure (figure 13(b)) during the production of the planar carbon fibre composite panel in which the EP2400 resin system was used. The degree of cure plotted in figure 13(b) was determined from the refractive index measured over the isothermal phase of figure 13(a), which started 54 min after the start of the experiment (indicated by the dotted line). Again, the noise in the Fresnel sensor signals in the early stage of the cure cycle (figure 13(a)) could be attributed to movement and bending of the sensor element within the preform, as perturbations of this part of the optical fibre down lead are not corrected by the intensity referencing.

5.2. FBG sensors

The cure process in the tail cone was also monitored using the embedded HiBi FBG and SM FBG sensors, which measured the transverse and longitudinal strains, respectively, developed during the chemical cure reaction. The HiBi FBG and SM FBG sensors were interrogated simultaneously using the instrumentation described in section 2. The spectra from the SM FBGs and HiBi FBGs did not exhibit peak splitting, which is a phenomenon usually associated with induced birefringence [58] or that, in some cases, is associated with non-uniform strain distributed spatially along the FBG [59]. The use of HiBi FBGs in this paper ensured that the peaks did not split from any induced birefringence.

5.2.1. Development of longitudinal strain.
Following the infusion of resin into the tail cone, the cure process was initiated by applying the cure thermal profile to the oven containing the tail cone. The longitudinal strains developed in the tail cone preform during the curing of the RTM6 resin were monitored using the embedded SM FBG sensors. Figure 14 shows the longitudinal strain measured by five SM FBG sensors embedded at locations S1–S5, from the exhaust to the fuselage end of the tail cone, in zone-F1 (figure 7). The information contained in figure 14 is interpreted in this paper as follows: the increase in the strain during the 'infusion phase' corresponds to the combined thermo-mechanical expansion [60, 61] of all the components of the tail cone, which includes the moulding tool, carbon-fibre and resin, while the subsequent decrease in the strain during the cure phase relates to shrinkage caused by the chemical cure reaction [60–62].

The sensor located at S1, closest to the exhaust end of the tail cone, detected strains of 428 ± 5 $\mu\varepsilon$ and -153 ± 5 $\mu\varepsilon$ as thermo-mechanical expansion and cure-induced shrinkage

Table 3. Summary of the longitudinal strains in the tail cone measured during the curing process by SM FBG sensors embedded at the various locations along the length of the tail cone. The numbering of the sensors, S1–S5, is from the exhaust end to the fuselage end of the tail cone.

SM FBG sensor locations	Thermo-mechanical expansion ($\mu\varepsilon$)	Cure-induced shrinkage ($\mu\varepsilon$)
S1	428 ± 5	-153 ± 5
S2	455 ± 4	-158 ± 4
S3	493 ± 4	-160 ± 4
S4	454 ± 4	-179 ± 4
S5	588 ± 4	-158 ± 4

respectively, measured in the longitudinal direction of the tail cone. The corresponding values measured by the SM FBG sensor located at S5, closest to the fuselage end of the tail cone were 588 ± 4 $\mu\varepsilon$ and -158 ± 4 $\mu\varepsilon$ respectively (figure 14). Figure 14 shows that cure-induced shrinkage in the longitudinal direction of the tail cone was detected ~140 min into the cure phase. A summary of the SM FBG sensor measurements of the longitudinal strains developed in the tail cone during the cure process is provided in table 3. The magnitudes of the longitudinal strains measured at the different locations of the tail cone are in good agreement with each other.

5.2.2. Development of transverse strain.
The polarisation Eigen-axes of the HiBi FBG sensors were aligned with the in-plane and out-of-plane directions of the tail cone, making it possible to monitor the out-of-plane transverse strains developed during the curing process [39, 40], as discussed in section 3. The temperature for the cure cycle, measured by thermocouple sensors embedded into the tail cone preform, was used together with a prior calibration for the temperature responsivity of the Bragg peaks [41] to compensate for the influence of temperature on the measured Bragg wavelengths, as discussed in section 2.2. The effective transverse strain was calculated using equation (5) [39].

Figure 15 shows the effective transverse strain measured by the five HiBi FBG sensors embedded at the locations S1–S5, from the exhaust to the fuselage end of the tail cone, in zone-F1 (figure 7). Again it is proposed that the increase in the effective transverse strain during the 'infusion phase' corresponds to the combined thermo-mechanical expansion [60, 61] of all the components of the tail cone, which include the moulding tool, carbon-fibre and resin, while the subsequent decrease in the effective transverse strain during the cure phase relates to shrinkage caused by the chemical cure reaction [60–63].

Figure 15 shows that the sensor located at S1, closest to the exhaust end of the tail cone, exhibited thermo-mechanical expansion and cure-induced shrinkage of 109 ± 10 $\mu\varepsilon$ and -1139 ± 10 $\mu\varepsilon$ respectively, in the through-the-thickness (i.e. out-of-plane) direction. Similarly, the sensor located at S5, closest to the fuselage end of the tail cone, detected strains of 516 ± 7 $\mu\varepsilon$ and -1252 ± 7 $\mu\varepsilon$ for the thermo-mechanical expansion and cure-induced shrinkage, respectively, measured in the through-the-thickness direction.
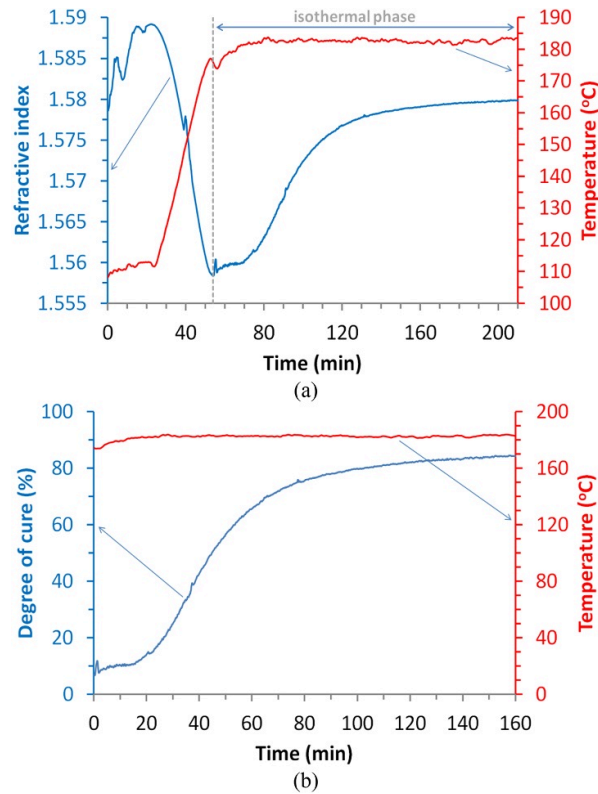
Figure 13. (a) Real-time monitoring of the refractive index of EP2400 resin using an embedded optical fibre Fresnel sensor during the curing of a planar carbon fibre reinforced composite in an industrial oven and (b) degree of cure monitored in real time by converting the refractive index measurement over the isothermal phase of (a), obtained by applying the correlation function (cubic) from the calibration of (b). The dotted line in (a) marks the time, 54 min, when the isothermal phase of the cure started, which corresponds to 0 min in (b). The final degree of cure is proportional to the curing temperature and dwell time at that temperature [55, 56]. As the isotherm dwell time in (b) is less than that employed during calibration (figure 12(a)), the degree of cure is only ~84% instead of 100%. Some researchers have suggested that the degree of cure for a reinforced resin might also differ from that of a neat resin [57].
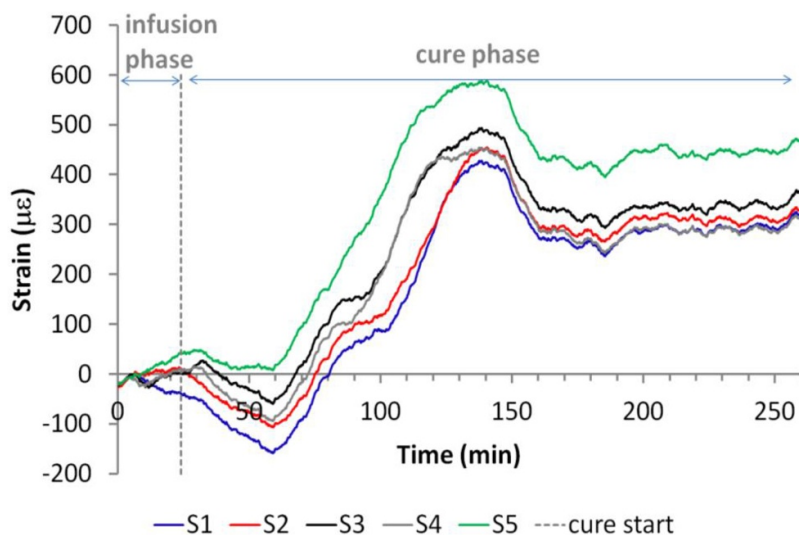

Figure 14. Longitudinal strain developed length-wise along the tail cone during the curing process, measured by SM FBG sensors embedded at sensor positions S1, S2, S3, S4 and S5 in zone-F1 of the tail cone (figure 7). The numbering of the sensors S1–S5 is from the exhaust end to the fuselage end of the tail cone.

The cure-induced shrinkage, through-the-thickness of the tail cone, is detected earlier in the curing phase than the cure-induced shrinkage exhibited by the longitudinal strain (shown in figure 14), confirming observations reported in [39], suggesting that this is a more sensitive measure of the start of the cure process. A summary of the HiBi FBG sensor measurements of the effective transverse strains developed through-the-thickness of the tail cone during the curing
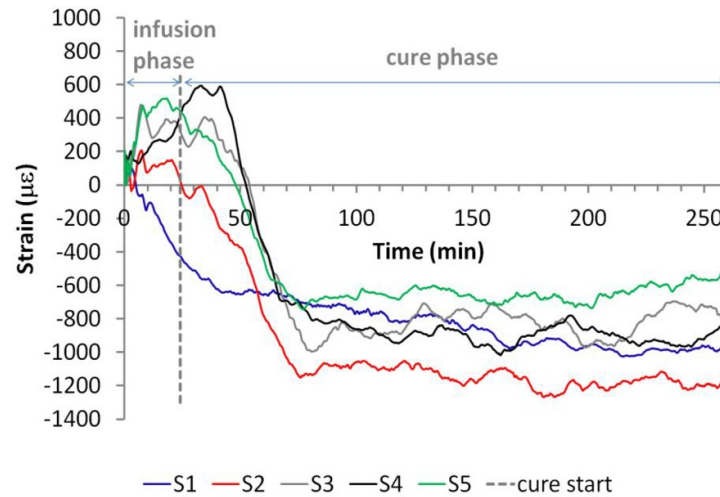
Figure 15. Transverse strain developed through-the-thickness of the tail cone during the curing process measured by HiBi FBG sensors embedded at sensor positions S1, S2, S3, S4 and S5 in Zone-F1 (figure 7). The numbering of the sensors, that is, S1–S5 is from the exhaust end to the fuselage end of the tail cone.

Table 4. Summary of the effective transverse strain through-the-thickness and directed out-of-plane of the tail cone measured during the curing process by HiBi FBG sensors embedded at various locations along the length of the tail cone. The numbering of the sensors, i.e. S1–S5 is from the exhaust end to the fuselage end of the tail cone.

HiBi FBG sensor locations	Thermo-mechanical expansion (με)	Cure-induced shrinkage (με)
S1	109 ± 10	−1139 ± 10
S2	208 ± 15	−1476 ± 15
S3	480 ± 17	−1475 ± 17
S4	595 ± 13	−1612 ± 13
S5	516 ± 7	−1252 ± 7

process is provided in table 4, showing good agreement between measurements at the different locations of the tail cone. It should be noted that the cure-induced shrinkage in the longitudinal direction, recorded by the SM FBG sensors, was about nine times smaller than that detected in the transverse direction of the tail cone by HiBi FBG sensors. Cure-induced shrinkage strains, transverse to the reinforcing fibres and in the through-the-thickness direction, are known to be significantly greater than in the longitudinal or in-plane direction of the composite part [57, 64].

6. Post-fabrication mechanical testing

The embedded SM FBG and HiBi FBG sensors used to monitor the processes involved in the manufacture of the tail cone were used subsequently, along with surfaced-mounted resistance foil strain gauge (RFSG) rosettes, to monitor structural strains during post-fabrication pressure loading (figure 16). After the tail cone was manufactured, the RFSG sensors were bonded to the outer surface of the tail cone at locations close to where the FBG sensors were embedded. The RFSG rosette sensor at each location was configured

to measure longitudinal, shear and circumferential strains (figure 16(b)). Figure 16(b) describes the strain components measured by the FBG and RFSG sensors. The longitudinal strains measured by the SM FBG sensors were compared to those measured by the RFSG sensors. Figure 16(b) shows that the in-plane transverse strain measured by the HiBi FBG sensors is oriented in the same direction as the circumferential strain measured by the RFSG sensors, which allowed the comparison of the strains measured by the two types of sensors. The in-plane transverse strain was determined using equation (5) but with the order of subtraction in the parenthesis reversed. The interior surface of the tail cone was lined with vacuum bags to allow the tail cone to be subjected to vacuum pressure loading. Aluminium foil was used to seal the window and door areas as shown in figure 16(a).

6.1. Transverse strain

The in-plane transverse strains and the circumferential strains monitored by the embedded HiBi FBG and surfaced-mounted RFSG sensors, respectively, midway along the length of the tail cone at sensor location S3 (figure 7) were compared around the tail cone in zones F1 F2, F3 and F4 (figure 17). The general trend and the sign of the strains measured by the embedded HiBi FBG and surfaced-mounted RFSG sensors were in good agreement. Figure 17 shows that the trend in the measured strain varies from one sensor position to the next, midway around the tail cone, which was expected due to the complex structure of the tail cone that consisted of a distribution of 10 stringers, tufting zones, different ply-orientation architecture, windows, doors, and non-uniform dimensions. Differences in the measurements by the two sensor types were likely caused by the differences in the loadings experienced by the *embedded* HiBi FBG sensors and the *surface*-bonded RFSG sensors. Some HiBi FB sensors in figure 17 did not record 0 με after unloading of the vacuum pressure, suggesting that the tail cone remained distorted.
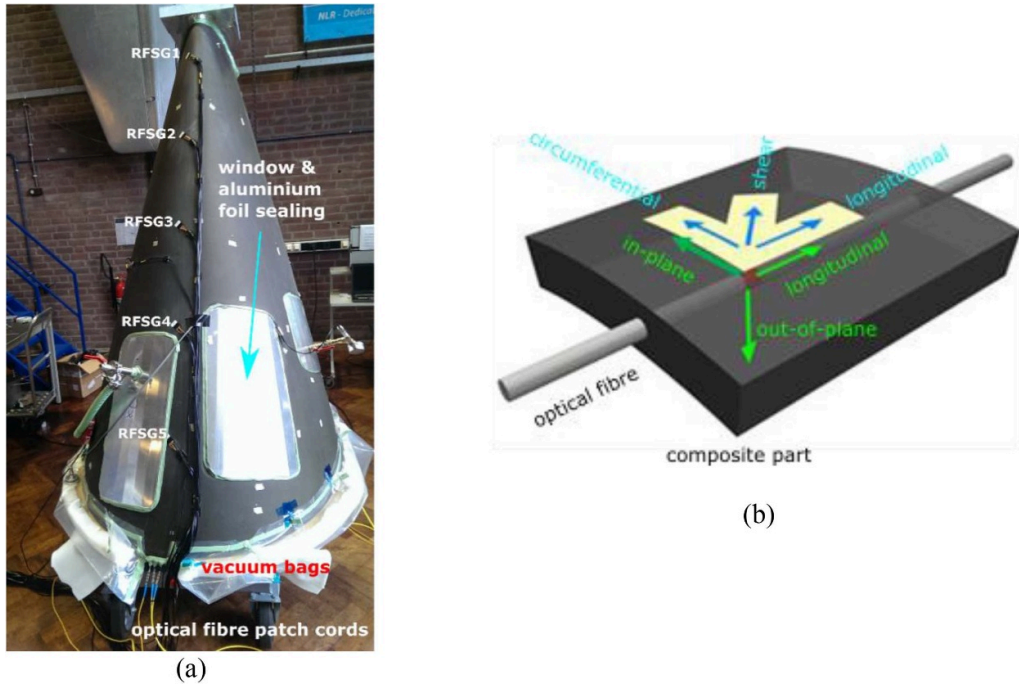
Figure 16. (a) Tail cone configuration for the vacuum loading tests in which aluminium foils and plates were used to seal the window and door areas. (b) Strain components measured by the embedded FBG (green arrows) sensors and surface-mounted RFSG (blue arrows) rosette sensors. The in-plane and out-of-plane transverse strains were measured by the HiBi FBG sensor while the longitudinal strain was measured by the SM FBG sensor embedded adjacently.
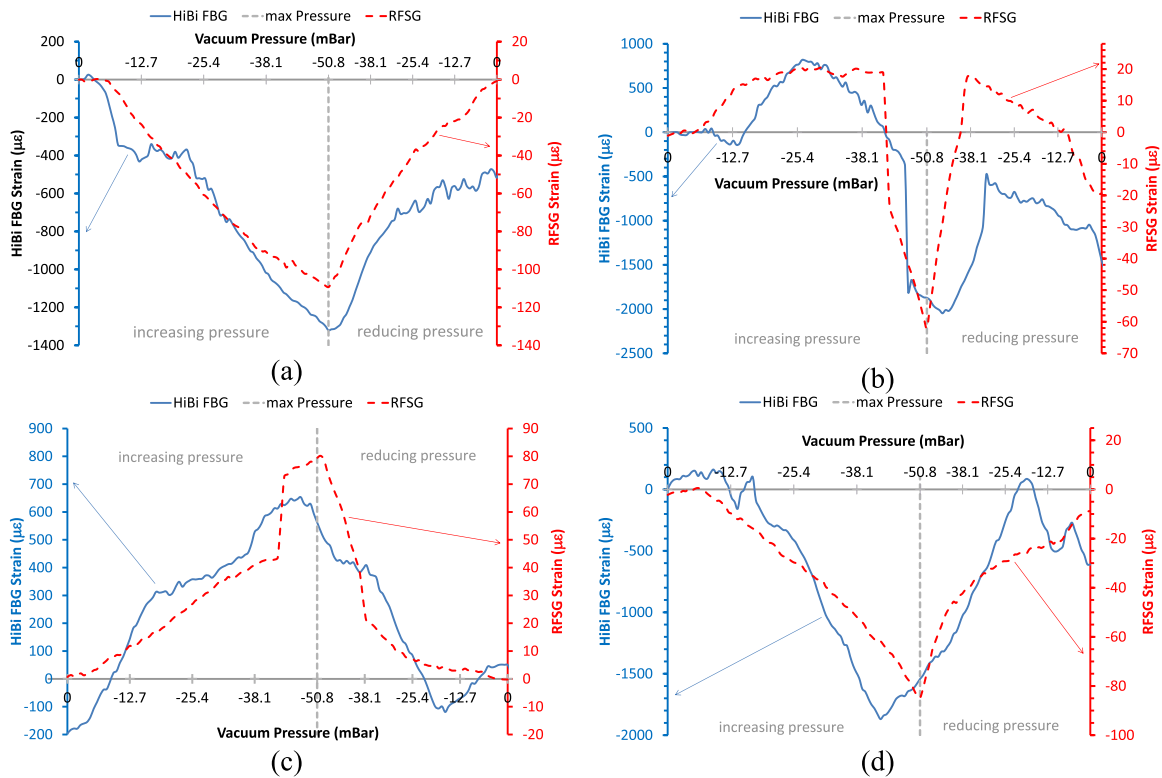

Figure 17. Comparison of the in-plane transverse and circumferential strains measured by the embedded HiBi FBG and the surface-mounted RFSG sensors, respectively, measured at sensor position S3 in (a) zone-F1, (b) zone-F2, (c) zone-F3 and (d) zone-F4 of the tail cone (figure 7).
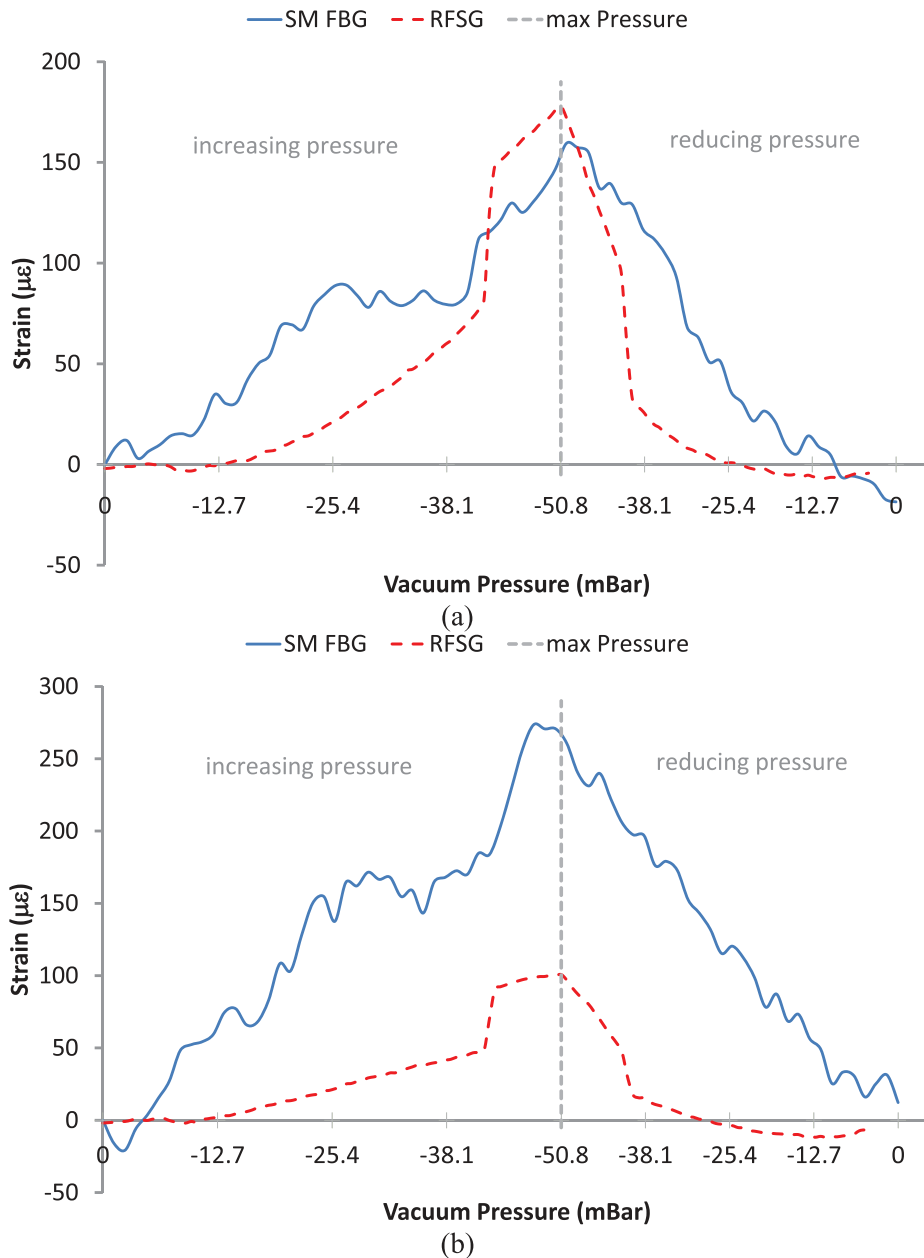
Figure 18. Comparison of the embedded SM FBG and surface-mounted RFSG sensors longitudinal strain measurements in zone-F3 (figure 7) of the tail cone at sensor location (a) S4 and (b) S5.

6.2. Longitudinal strain

Figure 18 compares the longitudinal strains measured by the embedded SM FBG sensors and the surface-mounted RFSG sensors in zone-F3 (figure 7) of the tail cone at neighbouring sensor locations S4 and S5. The SM FBG and RFSG sensors at sensor location S4 measured maximum longitudinal strains of 160 ± 4 με and 178 με respectively, showing close agreement (figure 18(a)). The corresponding maximum longitudinal strains measured at sensor location S5 were 274 ± 4 με and 100 με for the SM FBG and RFSG sensors, respectively (figure 18(b)). The difference in the two measurements suggests that local loading within the tail cone is representative of flexion loading, which leads to variation of loads through-the-thickness of the tail cone.

7. Conclusion

The industrial manufacturing processing of a large, one-piece, full-scale all-carbon fibre composite aircraft tail cone assembly was monitored successfully using embedded optical fibre sensors, from carbon-fibre preform lay-up through production to post-fabrication mechanical testing. The processes monitored by the optical fibre sensors included strain and bending moments developed in the needle during tufting (published separately in [18, 32]), resin infusion, degree of cure of resin, longitudinal and transverse components of strain developed during cure and post-fabrication structural loading. This work reinforced the significance of optical fibre sensors, which are embeddable within fibre-reinforced composites, in providing an entire monitoring solution to the composite

manufacturing processes through to post-production structural testing, currently not possible from other sensor types, particularly in industrial manufacturing. The embedded sensors could be utilised for both quality control in manufacturing and for structural integrity assessment in post-manufactured parts as well as for health and usage monitoring in service. Process monitoring technology could be used to facilitate optimised production methodologies and to aid the modelling of advanced composites. Future developments will be required to produce miniaturised ingress/egress connectors for use with embedded optical fibre sensors. This is a clear example of an application in which the small dimensions of the optical fibre facilitate measurements that are not possible using other technologies.

Acknowledgments

ORCID iD

Ralph P Tatam https://orcid.org/0000-0001-9599-3639

References

[1] Deobald L, Park C Y, Desai N, Ramnath M, Jin O, Lucaszewicz D and Kerscher S 2014 Simulation of composite manufacturing variations to determine stiffness and strength reductions in automotive and aerospace structure *Proc. American Soc. for Compos., 29th Tech. Conf. Compos. Mater.* pp 166–84

[2] Konstantopoulos S, Fauster E and Schledjewski R 2014 Monitoring the production of FRP composites: a review of in-line sensing methods *Express Polym. Lett.* **8** 823–40

[3] Skordos A A, Karkanas P I and Partridge I K 2000 A dielectric sensor for measuring flow in resin transfer moulding *Meas. Sci. Technol.* **11** 25–31

[4] Hegg M C, Ogale A, Mescher A, Mamishev A and Minaie B 2005 Remote monitoring of resin transfer molding processes by distributed dielectric sensors *J. Compos. Mater.* **39** 1519–39

[5] Garschke C, Weimer C, Parlevliet P P and Fox B L 2012 Out-of-autoclave cure cycle study of a resin film infusion process using *in situ* process monitoring *Compos.* A **43** 935–44

[6] Schmachtenberg E, Schulte Z H J and Topker J 2005 Application of ultrasonics for the process control of resin transfer moulding (RTM) *Polym. Test.* **24** 330–8

[7] Tuncol G, Danisman M, Kaynar A and Sozer E M 2007 Constraints on monitoring resin flow in the resin transfer molding (RTM) process by using thermocouple sensors *Composites* A **38** 1363–86

[8] Xin C, Gu Y, Li M, Li Y and Zhang Z 2011 Online monitoring and analysis of resin pressure inside composite laminate during zero-bleeding autoclave process *Polym. Compos.* **32** 314–23

[9] Kosaka T, Ueda D, Ohsaka K and Sawada Y 2007 Cure monitoring of UV chain curing polymer by fiber optic measurement of refractive index *Proc. Int. Conf. Compos. Mater. (ICCM16)* (*Kyoto, Japan*) Paper No. MoBM1-3 (https://www.iccm-central.org/Proceedings/ICCM16proceedings/contents/pdf/MonB/MoBM1-03ge_kosakat224773p.pdf)

[10] Buggy S J, Chehura E, James S W and Tatam R P 2007 Optical fibre grating refractometers for resin cure monitoring *J. Opt.* A **9** S60–S65

[11] Keulen C, Yildiz M and Suleman A 2011 Multiplexed FBG and etched fiber sensors for process and health monitoring of 2-&-3-D RTM components *J. Reinf. Plast. Compos.* **30** 1055–64

[12] Takeo T and Hattori H 1982 Optical fiber sensor for measuring refractive index *Japan. J. Appl. Phys.* **21** 1509–12

[13] Kumar A, Subrahmanyam T V B, Sharma A D, Thyagarajan K, Pal B P and Goyal I C 1984 Novel refractometer using a tapered optical fibre *Electron. Lett.* **20** 534–5

[14] Jarzebinska R, Chehura E, James S W and Tatam R P 2012 Multiplexing a serial array of tapered optical fibre sensors using coherent optical frequency domain reflectometry *Meas. Sci. Technol.* **23** 105203

[15] Chan C-F, Ferrier G A, Thomson D J, Chen C, Albert J, Vincelette A and Lefebvre P 2007 Side-polished and tilted fiber Bragg grating sensors for structural health monitoring applications *Proc. SPIE* **6530** 65300F

[16] Kim C B and Su C B 2004 Measurement of the refractive index of liquids at 1.3 and 1.5 micron using a fibre optic Fresnel ratio meter *Meas. Sci. Technol.* **15** 1683–6

[17] Wang P, Molimard J, Drapier S, Vautrin A and Minni J C 2012 Monitoring the resin infusion manufacturing process under industrial environment using distributed sensors *J. Compos. Mater.* **46** 691–706

[18] Dell'Anno G, Partridge I, Cartie D, Hamlyn A, Chehura E, James S and Tatam R 2012 Automated manufacture of 3D reinforced aerospace composite structure *Struct. Integrity* **3** 22–40

[19] Xu W, Huang X G and Pan J S 2013 Simple fiber-optic refractive index sensor based on Fresnel reflection and optical switch *IEEE Sens. J.* **13** 1571–4

[20] Archer E, Broderick J and McIlhagger A T 2014 Internal strain measurement and cure monitoring of 3D angle interlock woven carbon fibre composites *Composites* B **56** 424–30

[21] O'Dwyer M J, Maistros G M, James S W, Tatam R P and Partridge I K 1998 Relating the state of cure to the real-time internal strain development in a curing composite using in-fibre Bragg gratings and dielectric sensors *Meas. Sci. Technol.* **9** 1153–8

[22] Chehura E, Jarzebinska R, Da Costa E F R, Skordos A A, James S W, Partridge I K and Tatam R P 2013 Multiplexed fibre-optic sensors for monitoring resin infusion, flow, and cure in composite material processing *Proc. SPIE* **8693** 86930F

[23] Wong R Y N, Chehura E, James S W and Tatam R P 2017 Resin directional flow and degree of cure sensing using chirped optical fiber long period gratings *IEEE Sens. J.* **17** 6605–14

[24] Yan B *et al* 2019 Temperature self-compensated refractive index sensor based on fiber Bragg grating and the ellipsoid structure *Sensors* **19** 5211

[25] Ling Q, Gu Z and Gao K 2018 Smart design of a long-period fiber grating refractive index sensor based on dual-peak resonance near the phase-matching turning point *Appl. Opt.* **57** 2693–7

[26] Chehura E, James S W and Tatam R P 2007 Temperature and strain discrimination using a single tilted fibre Bragg grating *Opt. Comm.* **275** 344–7

[27] Wang Q, Xia J, Zhao Y, Liu X, Wang P, Zhang Y-N, Sang C and Wang L 2014 Simultaneous measurement of strain and temperature with polarization maintaining fiber Bragg grating loop mirror *Instrum. Sci. Technol.* **42** 298–307

[28] Enríquez D a C, da Cruz A R and Giraldi M T M R 2012 Hybrid FBG–LPG sensor for surrounding refractive index and temperature simultaneous discrimination *Opt. Laser Technol.* **44** 981–6

[29] Shu X, Gwandu B A L, Liu Y, Zhang L and Bennion I 2001 Sampled fiber Bragg grating for simultaneous refractive-index and temperature measurement *Opt. Lett.* **26** 774–6

[30] Nair A K, Machavaram V R, Mahendran R S, Pandita S D, Paget C, Barrow C and Fernando G F 2015 Process monitoring of fibre reinforced composites using a multi-measurand fibre-optic sensor *Sens. Actuators* B **212** 93–106

[31] Mahendran R S, Wang L, Machavaram V R, Pandita S D, Chen R, Kukureka S N and Fernando G F 2009 Fiber-optic sensor design for chemical process and environmental monitoring *Opt. Lasers Eng.* **47** 1069–76

[32] Chehura E, Dell'Anno G, Huet T, Staines S, James S W, Partridge I K and Tatam R P 2014 On-line monitoring of multi-component strain development in a tufting needle using optical fibre Bragg grating sensors *Smart Mater. Struct.* **23** 075001 (9pp)

[33] Dell'Anno G, Treiber J W D and Partridge I K 2016 Manufacturing of composite parts reinforced through-thickness by tufting *Robot. Comput. Integr. Manuf.* **37** 262–72

[34] Giraldo C M, Sagredo J Z, Gomez J S and Corredera P 2017 Demonstration and methodology of structural monitoring of stringer runs out composite areas by embedded optical fiber sensors and connectors integrated during production in a composite plant *Sensors* **17** 1683

[35] Ramakrishnan M, Rajan G, Semenova Y and Farrell G 2016 Overview of fiber optic sensor technologies for strain/temperature sensing applications in composite materials *Sensors* **16** 99

[36] Born M and Wolf E 1999 *Principles of Optics* 7th (expanded) edn (Cambridge: Cambridge University Press)

[37] Dimopoulos A, Buggy S J, Skordos A A, James S W, Tatam R P and Partridge I K 2009 Monitoring cure in epoxies containing carbon nanotubes with an optical-fiber Fresnel refractometer *J. Appl. Polym. Sci.* **113** 730–5

[38] Dockney M L, James S W and Tatam R P 1996 Fibre Bragg gratings fabricated using a wavelength tuneable laser source and a phase mask based interferometer *Meas. Sci. Technol.* **7** 445–8

[39] Chehura E, Skordos A A, Ye C-C, James S W, Partridge I K and Tatam R P 2005 Strain development in curing epoxy resin and glass fibre/epoxy composites monitored by fibre Bragg grating sensors in birefringent optical fibre *Smart Mater. Struct.* **14** 354–62

[40] Chehura E, Buggy S J, James S W, Johnstone A, Lakrimi M, Domptail F, Twin A and Tatam R P 2011 Multi-component strain development in superconducting magnet coils monitored using fibre Bragg grating sensors fabricated in highly linearly birefringent fibre *Smart Mater. Struct.* **20** 125004

[41] Chehura E, Ye C-C, Staines S E, James S W and Tatam R P 2004 Characterization of the response of fibre Bragg gratings fabricated in stress and geometrically induced high birefringence fibres to temperature and transverse load *Smart Mater. Struct.* **13** 888–95

[42] Ye C-C, Staines S E, James S W and Tatam R P 2002 A polarization-maintaining fibre Bragg grating interrogation system for multi-axis strain sensing *Meas. Sci. Technol.* **13** 1446–9

[43] Lawrence C M, Nelson D V, Udd E and Bennett T 1999 A fibre optic sensor for transverse strain measurement *Exp. Mech.* **39** 202–9

[44] Chehura E, James S W, Staines S, Groenendijk C, Cartie D, Portet S, Hugon M and Tatam R P 2015 Monitoring the manufacturing process and the mechanical performance of a full-sized all carbon fibre composite tail cone assembly using embedded fibre optic sensors *Proc. Int. Conf. Compos. Mater. (ICCM20)* (*Copenhagen, Denmark*) P-ID 4220-3 http://www.iccm-central.org/Proceedings/ICCM20proceedings/papers/paper-4220-3.pdf)

[45] Leng J S and Asundi A 2002 Real-time cure monitoring of smart composite materials using extrinsic Fabry–Perot interferometer and fiber Bragg grating sensors *Smart Mater. Struct.* **11** 249–55

[46] Groves R M, Chehura E, Li W, Staines S E, James S W and Tatam R P 2007 Surface strain measurement: a comparison of speckle shearing interferometry and optical fibre Bragg gratings with resistance foil strain gauges *Meas. Sci. Technol.* **18** 1175–84

[47] Kashyap R 1999 *Fiber Bragg Gratings* (London: Academic Press)

[48] Coriolis Composites. Automated Dry Fibre Placement Machines technical information. [Online] 2000 [Cited: May 19, 2020.] (http://www.coriolis-composites.com/)

[49] Jennise T T T, Yuhazri M Y, Sihombing H, Yahaya S H, Nirmal U and Megat-Ahmad M M H 2013 Gravity effects of curing angle on laminated composite structures: a review on novel study *Adv. Mater. Sci. Eng.* **2013** 876824

[50] Zhao C and Zhang G 2012 Effect of gravity on resin flow behaviour by VARI process *Adv. Mater. Res.* **557–9** 1471–4

[51] Galy J, Sabra A and Pascault J-P 1986 Characterization of epoxy thermosetting systems by differential scanning calorimetry *Polym. Eng. Sci.* **26** 1514–23

[52] Lee W I, Loos A C and Springer G S 1982 Heat of reaction, degree of cure and viscosity of Hercules 3501-6 resin *J. Compos. Mater.* **16** 510–20

[53] Solvay Composite Materials 2017 Prism™ EP2400 resin system for infusion *Technical Data Sheet* TDS Prism EP2400_2017_01_12

[54] Rodriguez-Lence F, Munoz-Esquer P, Menendez J M, Pardo de Vera C, Diaz S and Guemes J A 1999 Smart sensors for resin flow and composite cure monitoring *Proc. Int. Conf. Compos. Mater. (ICCM12)* (*Paris, France*) Paper No. 1100 http://iccm-central.org/Proceedings/ICCM12proceedings/site/papers/pap1100.pdf

[55] Dong A, Zhao Y, Zhao X and Yu Q 2018 Cure cycle optimization of rapidly cured out-of-autoclave composites *Materials* **11** 421–35

[56] Epoxy Technologies Inc. 2020 Cure Matters Determining the proper cure schedule *Technical Note* EPO-113-01

[57] Minakuchi S 2015 *In situ* characterization of direction-dependent cure-induced shrinkage in thermoset composite laminates with fiber-optic sensors embedded in through-thickness and in-plane directions *J. Compos. Mater.* **49** 1021–34

[58] Gafsi R and Mahmoud El-Sherif A 2000 Analysis of induced-birefringence effects on fiber Bragg gratings *Opt. Fiber Technol.* **6** 299–323

[59] Ling H-Y , Lau K-T , Cheng L and Chow K-W 2005 Embedded fibre Bragg grating sensors for non-uniform strain sensing in composite structures *Meas. Sci. Technol.* **16** 2415–24

[60] Khoun L, Oliveira R-D, Michaud V and Hubert P 2011 Investigation of process-induced strains development by

fibre Bragg grating sensors in resin transfer moulded composites *Composites* A **42** 274–82

[61] Harsch M, Karger-Kocsis J and Herzog F 2008 Monitoring of cure-induced strain of an epoxy resin by fiber Bragg grating sensor *J. Appl. Polym. Sci.* **107** 719–25

[62] Robert L and Dusserre G 2014 Assessment of thermoset cure-induced strains by fiber Bragg grating sensor *Polym. Eng. Sci.* **54** 1585–94

[63] Chiesura G, Lamberti A, Yang Y, Geert L, Paepegem W V, Steve V, Vanfleteren J and Degrieck J 2016 RTM production

monitoring of the A380 hinge arm droop nose mechanism: a multi-sensor approach *Sensors* **16** 886

[64] Tezvergil A, Lassila L V J and Vallittu P K 2006 The effect of fiber orientation on the polymerization shrinkage strain of fiber-reinforced composites *Dental Mater.* **22** 610–16

[65] European Union FP7 2009 ADVance Integrated composite TailCone (ADVITAC) *Programme Fact Sheet* (http://cordis.europa.eu/project/rcn/91195/en) (Accessed :19 May 2020)